QUT Digital Repository:
http://eprints.qut.edu.au/

QUT

This is the author version published as:

GPS Fault Detection with IMU and Aircraft Dynamics

T. S. Bruggemann, D. G. Greer and R. A. Walker, *Member, IEEE*

Abstract— **Approaches with Vertical Guidance (APV) can provide greater safety and cost savings to general aviation through accurate GPS horizontal and vertical navigation. However, GPS needs augmentation to achieve APV fault detection requirements. Aircraft Based Augmentation Systems (ABAS) fuse GPS with additional sensors at the aircraft. Typical ABAS designs assume high-quality inertial sensors with Kalman filters but these are too expensive for general aviation.**

Instead of using high-quality (and expensive) sensors, the purpose of this paper is to investigate augmenting GPS with a low-quality MEMS IMU and Aircraft Dynamic Model (ADM). The IMU and ADM are fused together using a multiple model fusion strategy in a bank of Extended Kalman Filters (EKF) with the Normalized Solution Separation (NSS) fault detection scheme. A tightly-coupled configuration with GPS is used and frequent GPS updates are applied to the IMU and ADM to compensate for their errors.

Based upon a simulated APV approach, the performance of this architecture in detecting a GPS ramp fault is investigated showing a performance improvement over a GPS-only implementation "snapshot" implementation of the NSS method. The effect of fusing the IMU with the ADM is evaluated by comparing a GPS-IMU-ADM EKF with a GPS-IMU EKF where a small improvement in protection levels is shown.

T. S. Bruggemann is with the Australian Research Centre for Aerospace Automation (ARCAA) at Queensland University of Technology (QUT) (phone:+61-7-3138-1362;e-mail: t.bruggemann@qut.edu.au).

D. G. Greer is with the Australian Research Centre for Aerospace Automation (ARCAA) at Queensland University of Technology (QUT) (phone:+61-7-3138-1362;e-mail: d.greer@qut.edu.au).

Prof R. A. Walker is Director of the Australian Research Centre for Aerospace Automation (ARCAA) at Queensland University of Technology (QUT) (phone:+61-7-3138-1772;e-mail: ra.walker@qut.edu.au)

Index Terms—aircraft dynamics, aircraft navigation, Global Positioning System, inertial navigation, fault detection.

I. INTRODUCTION

In general aviation, Approaches with Vertical Guidance (APV) allow greater safety and cost savings through accurate GPS-provided horizontal and vertical navigation. However, GPS needs augmentation to achieve stringent APV fault detection requirements [1]. Aircraft Based Augmentation Systems (ABAS) fuse GPS with additional sensors at the aircraft. Typical designs such as in the AIME [2], Multiple Solution Separation [3] and Normalized Solution Separation (NSS) methods [4], assume an accurate inertially-derived reference trajectory with Kalman filters. However, high-quality inertial sensors are too expensive for general aviation.

Instead of using high-quality (but expensive) sensors, the purpose of this paper is to investigate augmenting GPS with a low-cost and low-quality MEMS IMU and Aircraft Dynamic Model (ADM). In this approach, rather than using Kalman filters in an open-loop configuration, the IMU and ADM are fused together in a bank of Extended Kalman Filters (EKF) in closed-loop configuration. Frequent GPS updates are applied to the IMU and ADM to compensate for their errors, and a tightly-coupled configuration is adopted. To exploit the inclusion of the aircraft dynamics, the IMU and ADM are fused together using a multiple model fusion strategy. For fault detection the NSS method is adopted. This new architecture concept is termed the GPS-IMU-ADM EKF.

The concept of using aircraft dynamics in navigation is not new. In the available literature it was studied for improving inertial coasting and enhancing the robustness of the navigation solution in [5], [6] and single GPS antenna attitude determination in [7]. In contrast to these applications, the use of aircraft dynamics in GPS fault detection is investigated here. The incorporation of additional information into the system such as aircraft dynamics, may allow greater confidence in the state estimates leading to improved GPS fault detection performance.

This paper is structured as follows. After describing the GPS-IMU-ADM EKF architecture concept in section II, the ADM is presented in section III as well as descriptions of the EKF with Multiple Model Fusion (MMF) and the NSS method. Section IV presents simulations which evaluate the fault detection performance of the GPS-IMU-ADM EKF and compare against a GPS-IMU EKF and GPS-only "snapshot" implementation, for a general aviation aircraft on APV approach. Firstly, the simulation environment test setup is described where typical GPS, IMU, ADM and environmental errors are considered. Then, the ability to detect a 0.5 m/s ramp fault on a GPS pseudorange measurement is investigated, by comparing protection levels and time to fault detection of the GPS-IMU-ADM EKF, GPS-IMU EKF and GPS-only implementation. Finally, a comparison in protection levels over different satellite geometries in a day is made for the GPS-IMU-ADM EKF , GPS-IMU EKF and GPS-only implementations.

One potential use for lower-cost ABAS with low-cost IMU and aircraft dynamics, may be to enhance existing GPS-only fault detection solutions or help overcome deficiencies in existing augmentation systems for general aviation. Whilst countries such as the USA have the Wide Area Augmentation System (WAAS), countries such as Australia for example cannot justify such costs and currently do not have an augmentation solution of their own for the general aviation community. Less expensive concepts such as the Ground-based Regional Augmentation System (GRAS) have been proposed [8] which use ground-based VHF line-of-sight transmissions to aircraft instead of geostationary satellites as in WAAS. GRAS has limitations however – for example the GRAS transmissions may be blocked due to surrounding terrain, depending upon aircraft altitude and proximity to the GRAS data broadcast station. This could be because GRAS broadcast stations are unable to be placed at optimal locations to achieve complete coverage for cost reasons or site restrictions such as difficult terrain [8]. In a sparsely populated and vast country such as Australia, there may also be regional areas which do not have GRAS service availability. In these cases, lower-cost ABAS consisting of low-cost IMU and other information such as aircraft dynamics, may provide the necessary GPS augmentation.

II. GPS-IMU-ADM EKF Architecture Description

Fig. 1 shows the GPS-IMU-ADM EKF architecture concept. It consists of a GPS, IMU, ADM, a bank of EKFs and the Normalized Solution Separation (NSS) Fault Detection (FD) scheme. The main difference between this approach and others [2], [3], [4] is the use of EKFs, low quality IMU, aircraft dynamics and a closed-loop configuration. Because low-quality MEMS inertial sensors are not meant for coasting [9] frequent GPS updates are required. This is also required for the ADM which has an accuracy no better than the IMU. Therefore in this approach "coasting" is neglected.

The Normalized Solution Separation (NSS) method [4] relies upon one filter using all N satellites in view termed the "full-filter" and N "sub-filters" which use $N-1$ satellites. Each sub-filter has a different satellite omitted from its solution than the others allowing for detection of one satellite fault at a time. The solutions from the full-filter and sub-filters are then used by the NSS algorithm to determine whether there is a position fault or not. If no fault is detected the IMU accelerometer and gyroscope biases and GPS receiver clock biases calculated by each filter are fed-back as indicated by the "corrections" block in Fig. 1. Each filter is corrected with the estimates from its own filter therefore there are $N+1$ filter corrections to the GPS and IMU components of the $N+1$ filters in the system. If a fault is detected, fault exclusion is the next step however a fault exclusion algorithm's performance with this architecture is not investigated in this paper and is left for further work.
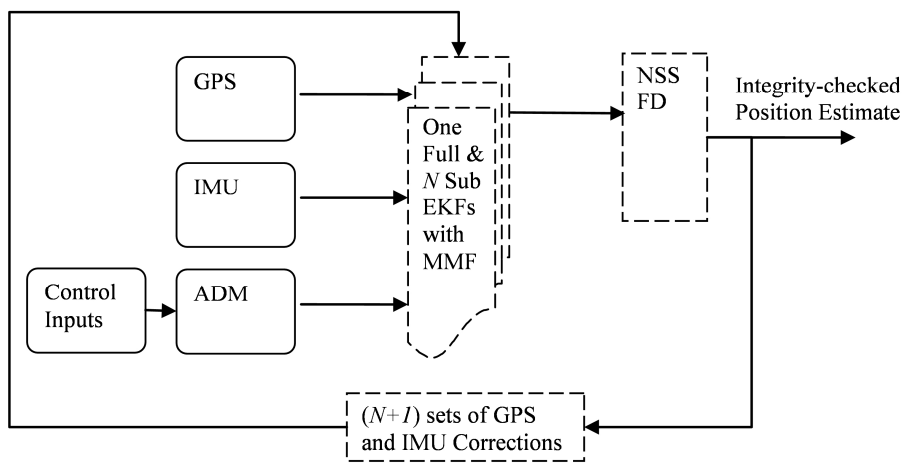
Fig. 1. The GPS-IMU-ADM EKF architecture concept.

III. AIRCRAFT DYNAMIC MODEL

The ADM consists of a set of coupled, nonlinear ordinary differential equations by which the aerodynamic forces and moments acting on the aircraft can be estimated [10]. These equations are a function of nondimensional aerodynamic coefficients, measured control surface deflections (aileron, elevator, rudder) and aircraft states. From this aerodynamic knowledge the accelerations and angular rates of the vehicle are derived. Fig. 2 shows the body axes of the aircraft, x_b, y_b, z_b with origin at the centre of gravity. p, q, r are the angular velocities, u, v, w are the body velocities, X, Y, Z are the aerodynamic forces and L, M, N are the aerodynamic moments as per standard nomenclature [11].
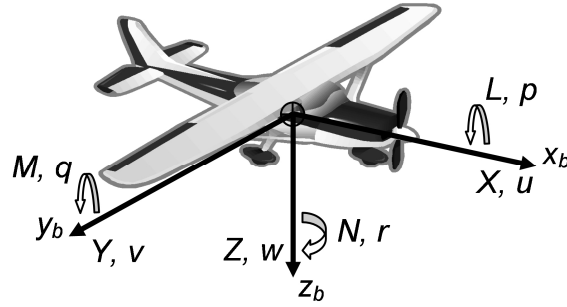

Fig. 2. Aircraft body axes, showing the location and direction of the aircraft's body accelerations, angular rates, aerodynamic forces and moments.

The angular accelerations in rad/s^2 are

$$\dot{p} = (c_1 r + c_2 p)q + c_3 L + c_4 N \qquad (1)$$

$$\dot{q} = c_5 pr - c_6 (p^2 - r^2) + c_7 M \qquad (2)$$

$$\dot{r} = (c_8 p - c_2 r)q + c_4 L + c_9 N \qquad (3)$$

where c1 to c8 are inertial coefficients [10].

The body-axis accelerations in m/s^2 are

$$\dot{u} = rv - qw - g\,sin(\theta) + X / m \qquad (4)$$

$$\dot{v} = pw - ru + g\,sin(\phi)cos(\theta) + Y / m \qquad (5)$$

$$\dot{w} = qu - pv + g\,cos(\phi)cos(\theta) + Z / m \qquad (6)$$

where ϕ, θ are roll, pitch attitude, g is gravity and m is the mass of the aircraft. From these the position, velocity and attitude of the aircraft are derived. The following section explains how the IMU and ADM information are fused together in the EKFs with Multiple Model Fusion (MMF).

A. EKF with Multiple Model Fusion

The process model of an EKF provides a prediction of the states of the vehicle based on past measurements. The model predicts the state of the vehicle and the GPS measurements are used to update the prediction. This may provide greater performance than standalone GPS. In the system described in Fig. 1 there are two process models – one for the IMU and one for the ADM. The IMU process model is the mechanization equations used to derive the aircraft attitude, velocity and position from accelerometer and gyroscope measurements [12]. The ADM process model is similar except it estimates the acceleration and angular rates of the vehicle from known aerodynamics given measured control inputs [10].

In this study the accuracy of the ADM angular rate and acceleration estimates was worse than the angular rate and acceleration measurements of the MEMS IMU as determined by comparing them when unaided by GPS, in simulation. However despite this the ADM may still provide useful and independent information about the system which may be exploited through an existing multiple model fusion strategy called Multiple Model Fusion (MMF) [13], [14].

In the EKF design there is one state vector for the IMU-derived estimates and another for the ADM-derived estimates. In the following equations the IMU is denoted by superscript I, the ADM by D and the GPS by G. The state vectors at discrete time k are

$$\chi_k^I = [\, q_0, q_1, q_2, q_3, v_N, v_E, v_D, l, \Lambda, h\,]^T \qquad (7)$$

$$\chi_k^D = [\, q_0, q_1, q_2, q_3, v_N, v_E, v_D, l, \Lambda, h\,]^T \qquad (8)$$

consisting of four attitude states q_0, q_1, q_2, q_3 (in quaternion representation), three velocity states v_N, v_E, v_D, (in North, East, Down coordinate frame), latitude, longitude and height, l, Λ, h.

The state is augmented with extra terms to account for GPS and IMU errors. The state vector containing the augmented states for the IMU is

$$\chi_{Ak}^{I} = [\ \Delta t, \Delta \dot{t}, \nabla a_x, \nabla a_y, \nabla a_z, \nabla p, \nabla q, \nabla r\ ]^{T} \qquad (9)$$

and for the ADM is

$$\chi_{Ak}^{D} = [\Delta t, \Delta \dot{t}]^{T} \qquad (10)$$

where Δt is GPS receiver clock bias, $\Delta \dot{t}$ is GPS receiver clock drift, ∇a_x, ∇a_y, ∇a_z are acceleration biases and ∇p, ∇q, ∇r are angular rate biases.

These are the corrections applied to the GPS and IMU in the feedback loop as indicated by the "corrections" block in Fig. 1. There is however a risk of unobservability by including six IMU biases [15] and the observability could be improved by including heading measurements from a compass for example as studied in [16]. The ADM could also be augmented with aerodynamic coefficients and wind states as in [5], however there are also observability issues associated with this approach.

To achieve MMF all the information is combined in a "combined filter" as indicated by superscript C in the following equations. The GPS-IMU-ADM EKF can be thought of as a GPS-IMU EKF stacked on top of a GPS-ADM EKF. The EKF operates on the state errors where the state error vector structure is

$$x_k^{C} = [x_k^{I}, x_k^{D}]^{T}. \qquad (11)$$

x_k^{I} is the IMU state error vector,

$$x_k^{I} = [\delta\Phi_N, \delta\Phi_E, \delta\Phi_D, \delta v_N, \delta v_E, \delta v_D, \delta l, \delta\Lambda, \delta h, \delta\chi_{Ak}^{I}]^{T} \qquad (12)$$

where $\delta\Phi_N, \delta\Phi_E$ are tilt errors with respect to the vertical and $\delta\Phi_D$ is azimuth (heading) error. $\delta v_N, \delta v_E, \delta v_D$ are velocity errors and $\delta l, \delta\Lambda, \delta h$ are latitude, longitude and height errors and $\delta\chi_{Ak}^{I}$ is a vector of augmented state errors. Similarly the ADM state error vector x_k^{D} is

$$x_k^{D} = [\delta\Phi_N, \delta\Phi_E, \delta\Phi_D, \delta v_N, \delta v_E, \delta v_D, \delta l, \delta\Lambda, \delta h, \delta\chi_{Ak}^{D}]^{T} \qquad (13)$$

Two state estimates are calculated by propagating the previous state using the IMU and ADM process models,

$$\chi_k^{I^-} = f(\chi_{k-1}^I, u_{k-1}^I, w_{k-1}^I) \tag{14}$$

$$\chi_k^{D^-} = f(\chi_{k-1}^D, u_{k-1}^D, w_{k-1}^D) \tag{15}$$

where u^I is the IMU measurements (accelerations, angular rates), u^D is the ADM control inputs and w^I and w^D are white noises. The combined state estimate vector is formed as

$$\chi_k^{C^-} = \left[\chi_k^{I^-}, \chi_{A^{k-1}}^{I^-}, \chi_k^{D^-}, \chi_{A^{k-1}}^{D^-}\right]^T. \tag{16}$$

The combined state error covariance is

$$P_k^{C^-} = \Phi_{k-1}^C P_{k-1}^C \Phi_{k-1}^{C^T} + Q_{k-1}^C \tag{17}$$

where Φ^C is the state transition matrix

$$\Phi_{k-1}^C = \begin{bmatrix} \Phi_{k-1}^I & 0 \\ 0 & \Phi_{k-1}^D \end{bmatrix}. \tag{18}$$

The process noise covariance matrix for the combined filter is

$$Q_{k-1}^C = \begin{bmatrix} Q_{k-1}^I & Q_{k-1}^{I-D} \\ Q_{k-1}^{D-I} & Q_{k-1}^D \end{bmatrix} \tag{19}$$

where

$$Q_{k-1}^I = \Phi_{k-1}^I G_{k-1}^I W_{k-1}^I G_{k-1}^{I^T} \Phi_{k-1}^{I^T} \Delta t^I \tag{20}$$

$$Q_{k-1}^D = \Phi_{k-1}^D G_{k-1}^D W_{k-1}^D G_{k-1}^{D^T} \Phi_{k-1}^{D^T} \Delta t^D. \tag{21}$$

G^I and G^D are design matrices for the IMU and ADM. W^I contains the expected noise statistics for the IMU and is a power spectral density matrix whose diagonal elements are the acceleration and angular rate noise variances of the IMU. W^D is a power spectral density matrix describing the magnitude of the process noise applied to the ADM attitude and velocity estimates to accommodate ADM uncertainties. W^I and W^D are tuned until the filters are consistent. Δt^I and Δt^D are the sample periods for the IMU and ADM.

Q^{I-D} and Q^{D-I} in (19) are the cross correlations between the IMU and ADM process noises. The IMU and ADM process noises will not be independent of each other due to the common assumptions and errors they share. As it is difficult to determine what the true correlation is it is treated as a tuning parameter for the filters where it is adjusted based on experience or empirical data.

With the GPS measurements a tightly coupled (pseudorange and pseudorange-rate) approach was taken. The measurements supplied to the filter are the difference between the GPS pseudorange and pseudorange-rates ρ^G, $\dot{\rho}^G$ and IMU and ADM state estimate-derived pseudorange and pseudorange-rates ρ^I, $\dot{\rho}^I$ and ρ^D, $\dot{\rho}^D$.

The measurement vectors of pseudoranges and pseudorange-rates are

$$z_k^I = \overline{\rho}_k^G - \overline{\rho}_k^I \tag{22}$$

$$z_k^D = \overline{\rho}_k^G - \overline{\rho}_k^D. \tag{23}$$

where

$$\overline{\rho}_k^G = \left[\rho_k^G, \dot{\rho}_k^G\right]^T \tag{24}$$

and similarly for $\overline{\rho}_k^I$ and $\overline{\rho}_k^D$.

Because the IMU and ADM process models can be thought of as virtual sensors whose output is a virtual measurement of the state of the vehicle based on all past time history [13], [14], the difference between the IMU and ADM process model's position estimates are presented to the combined filter as measurements,

$$z_k^{I-D} = \chi_k^{I^-}{}_{(l,\Lambda,h)} - \chi_k^{D^-}{}_{(l,\Lambda,h)}. \tag{25}$$

The measurements vector for the full-filter is

$$z_k^C = \left[z_k^I, z_k^{I-D}, z_k^D\right]^T. \tag{26}$$

The measurement noise covariance matrix is

$$R_k^C = \begin{bmatrix} R_k^G & 0 & R_k^G \\ 0 & R_k^{I-D} & 0 \\ R_k^G & 0 & R_k^G \end{bmatrix} \tag{27}$$

where R^C is a diagonal sub-matrix whose diagonal elements are the variances of the expected GPS pseudorange and pseudorange-rate noises. Because both IMU and ADM process models (14), (15) estimate the same state (position), the expected value of the difference of these (25) is zero with no uncertainty, so $R^{I-D} = 0$. This effectively applies hard constraints on the system [13]. In (27), note that R^C is singular. This is due to R^{I-D} being zero and the off-diagonal sub-matrices R^G which exist because the same GPS measurements are used to update the IMU and ADM state estimates. The singularity of R^C was overcome by applying the Moore-Penrose generalized inverse (pseudo-inverse) denoted as + in (29).

The state errors x_k^C are estimated as

$$x_k^C = K_k^C z_k^C \tag{28}$$

where the Kalman gain is

$$K_k^C = P_k^{C^-} H_k^{C^T} (H_k^C P_k^{C^-} H_k^{C^T} + R_k^C)^+ \tag{29}$$

and H_k^C is the measurements matrix.

The state update is

$$\chi_k^C = \chi_k^{C^-} + x_k^C \tag{30}$$

where

$$\chi_k^C = \begin{bmatrix} \chi_k^I, \chi_{Ak}^I, \chi_k^D, \chi_{Ak}^D \end{bmatrix}^T. \tag{31}$$

Finally, the corresponding state error covariance update is

$$\begin{aligned} P_k^C &= (I - K_k^C H_k^C) P_k^{C^-} (I - K_k^C H_k^C)^T \\ &\quad + K_k^C R_k^C K_k^{C^T} \end{aligned} . \tag{32}$$

The form of the EKF (7)-(32) is the same for all sub-filters however each of the N sub-filters use N-1

GPS pseudorange and *N-1* GPS pseudorange-rate measurements in (22)-(24). The full-filter and *N* sub-filters all propagate their own estimates using their own IMU and ADM process models (14), (15) and so are independent of each other. Therefore in the presence of a faulty measurement there will be one sub-filter that is free from the corrupting measurement fault.

After the update (30), (32) the state estimates χ_k^I and χ_k^D and their respective covariances in P_k^C are the same [13] and so either state estimates can be used for the fault detection. The position error covariances of P_k^I and P_k^D are expected to be smaller than they would be if an individual GPS-IMU EKF or GPS-ADM EKF were used due to the fusing of the ADM and IMU process models together by the EKF update equation (32). This is because (32) includes the cross-correlations between the IMU and ADM process models which serves to exploit information which is different about each process model. Only information which is independent between the process models is used to update the predictions [13], [14]. Both the IMU and the ADM process models are approximations to the true dynamics of the system and the source of the acceleration and angular rate information presented to each process is different and is corrupted by different error sources. For example, the IMU measurements of acceleration and angular rate contain errors (random noises and biases) due to the internal workings of the MEMS sensors. In contrast, the ADM has errors due to the assumptions made about the aircraft dynamics and the surrounding environment, imperfect knowledge of aerodynamic coefficients and noisy control surface measurements, for example. Fusing this different information together by MMF could result in better state estimates as compared to a GPS-IMU EKF which could result in improved GPS fault detection performance.

Although improved fault detection performance might be possible by including the ADM, one limitation is that this design is more complex than a GPS-IMU EKF. Another limitation is that the IMU and ADM are not independent which means that a fault or inconsistent filter with either of them will result in a fault being detected, yet, not being able to be distinguished from a GPS fault. Therefore to ensure robust performance the IMU and ADM reliability will need to be assured and the filters be consistent through filter tuning to limit the chance of filter divergence. Also the complexity of filter tuning may be a disadvantage of this system in a practical implementation. The following section will present the GPS fault detection procedure.

B. GPS Fault Detection Component

The fault detection algorithm must meet the ICAO requirements shown in Table I [17].

TABLE I
INTEGRITY MONITORING REQUIREMENTS

Performance Requirement	APV-I
Horizontal Accuracy (95%)	16 m
Vertical Accuracy (95%)	20 m
Integrity	$1\text{-}2 \times 10^{-7}$/h/approach
Horizontal Alert Limit (HAL)	40 m
Vertical Alert Limit (VAL)	50 m
Time To Alert	10 s
Availability	99 – 99.999%

At the algorithm level, two probabilities contribute to meeting the Integrity requirement in Table I; P_{md}, which is the probability of missed detection and P_{fd}, which is the probability of false detection. Fig. 3 shows the derivation of P_{md}. The probability of a GPS major service failure during the approach $P_{Failure}$ is 4.167×10^{-6} assuming there are three events per year with an average of eight visible satellites and the average time for an approach is 150 seconds [18].

$$P_{HMI} = 2 \times 10^{-7}\text{/approach}$$

Fault-free case H0, 1% of P_{HMI} allocated, $P_{H0} = 2 \times 10^{-9}$. 5% allocation for horizontal, $P_{H0\_H} = 1.0 \times 10^{-10}$. 95% allocation for vertical, $P_{H0\_V} = 1.9 \times 10^{-9}$.

Fault-in-progress case H1, 99% of P_{HMI} allocated, $P_{H1} = 1.98 \times 10^{-7}$. $P_{md} = P_{H1} / P_{Failure} = 0.0475$. 5% allocation for horizontal, $P_{md\_H} = 0.0025$. 95% allocation for vertical, $P_{md\_V} = 0.045$.
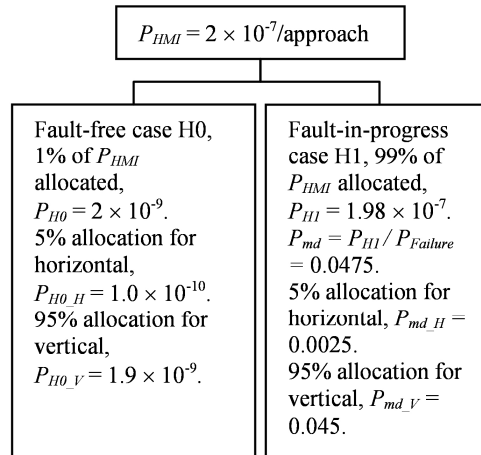
Fig. 3. Fault tree showing derivation of probabilities.

The requirement for the false detection probability is 1.6×10^{-5} per sample [19]. If the worst case scenario is assumed that there is only one independent sample per approach and an average approach time of 150 seconds, $P_{fd} = 1.06 \times 10^{-7}$.

1) Calculation of Test Statistic, Threshold and Protection Levels with the Normalized Solution Separation Method

The Normalized Solution Separation (NSS) method [4] was used for the fault detection method. Fault detection is by comparing calculated test statistics against a threshold, which are in the solution (position) domain. The test statistic is in the position domain. It is the separation in the horizontal position domain between full-set and sub-set solutions. For each sub-filter, the test statistic is

$$\lambda_{n_k} = \beta_{n_k}^T (B_{n_k}^{+}) \beta_{n_k} \tag{33}$$

where + indicates the Moore-Penrose generalized inverse. The solution separation vector between the full-filter solution and n^{th} sub-filter solution is:

$$\beta_{n_k} = \chi_{0_k} - \chi_{n_k} \tag{34}$$

where χ_{0_k} is the horizontal position vector from the full-filter and χ_{n_k} is the horizontal position vector of the sub-filter. The separation between the sub-filter and full-filter covariance estimates is:

$$B_{n_k} = P_{n_k} - P_{0_k} \tag{35}$$

where P_{n_k} is the horizontal component of P_k^c of the nth sub-filter and P_{0_k} is the horizontal component of P_k^c of the full-filter.

The detection threshold is determined using chi-square statistics to meet the required probability of false alert,

$$TD_n = f(\chi^2, P_{FA} / N) \tag{36}$$

where N is the number of available GPS measurements.

A fault is detected if

$$\sqrt{\lambda_n} > TD_n \tag{37}$$

for any sub-filter solution.

Yet before this takes place there must be confidence that the fault detection can satisfy P_{md}. If not, the integrity function is deemed to be unavailable and the system cannot be used for navigation, in accordance

with the requirements [19].

P_{md} is ensured by calculating a Horizontal Protection Level (HPL) which is the radius of a circle which bounds the true error with a probability of 1-P_{md} [18].

HPL_{H0} is for the fault free hypothesis H0 and calculated as

$$HPL_{H0k} = K_{H0}\sqrt{\sigma_{1,0}} \qquad (38)$$

where $\sigma_{1,0}$ is the maximum eigenvalue ($\sigma_{1,0} > \sigma_{2,0}$) of the full-filter covariance P_{0_k} and K_{H0} is a function of the 1-P_{H0_H} probability and $(\sigma_{2,0}/\sigma_{1,0})^{1/2}$ obtained from the Circular Error Probable (CEP) distribution [21].

HPL_{H1} is for the fault-in-progress hypothesis H1 and is calculated as:

$$HPL_{H1k} = \{ HPE_k^n \}_{MAX} \qquad (39)$$

where the total estimated horizontal position error for the nth sub-filter is

$$HPE_k^n = HPE\_B_k^n + HPE\_NP_k^n \\ - HPE\_NB_k^n \qquad . \qquad (40)$$

$HPE\_B_k^n$ is the horizontal position error due to bias and uncorrelated noise

$$HPE\_B_k^n = Pbias\sqrt{\sigma_{1,Bn}} \qquad (41)$$

where $\sigma_{1,Bn}$ is the maximum eigenvalue of the separation covariance B_{n_k}. $Pbias$ is the magnitude of the critical bias vector.

$$Pbias = \sqrt{\lambda} \qquad (42)$$

where λ is the noncentrality parameter of the noncentral χ^2 distribution which is determined to meet P_{md_H} and P_{fd}.

$HPE\_NP_k^n$ and $HPE\_NB_k^n$ are the Horizontal Position Errors due to noise only.

$$HPE\_NP_k^n = K_k^n\sqrt{\sigma_{1,n}} \qquad (43)$$

where $\sigma_{1,n}$ is the maximum eigenvalue of the sub-filter covariance P_{n_k} and K_k^n is function of 1-P_{md_H} probability and $(\sigma_{2,n}/\sigma_{1,n})^{1/2}$ from the CEP distribution.

$$HPE\_NB_k^n = K_{Bk}^n\sqrt{\sigma_{1,Bn}} \qquad (44)$$

where $K_{Bk}{}^n$ is a function of $1\text{-}P_{md\_H}$ probability and

$(\sigma_{2,Bn}/\sigma_{1,Bn})^{1/2}$ from the CEP distribution.

Finally,

$$HPL_k = \{ HPL_{H0k}, HPL_{H1k} \}_{MAX} \qquad (45)$$

and a similar process is followed for calculating VPL.

For fault detection the following conditions must be satisfied

$$HNSE_k < HPL_k < HAL \qquad (46)$$

$$VNSE_k < VPL_k < VAL \qquad (47)$$

Where HNSE is Horizontal Navigation System Error and VNSE is Vertical Navigation System Error. If the HPL exceeds the HAL then the fault detection function is deemed to be unavailable (in other words, it cannot be guaranteed that a fault can be detected within the P_{md}) and the navigation system cannot be used for navigation at that time. It is easy to see from (35) that HPL and VPL are dependant upon the state covariance of the full and sub-filters. This is where the MMF with an ADM may provide a lower state covariance leading to lower protection levels.

However, it should be noted that due to approximation of the true ranging errors with Gaussian statistics, the "tails" of the distribution may not have good representation (due to limited data) or found to be worse than Gaussian [27]. This will require conservative measures to be taken such as overbounding to offset optimistic results, leading to a corresponding increase in protection levels over the protection level results that will be presented in this paper. See [27] for further explanation of the problem and a potential solution to Gaussian over-bounding. Further work could be made in this area, which is beyond the scope of this paper.

IV. SIMULATION RESULTS

In order to evaluate the performance of the GPS-IMU-ADM EKF in fault detection a simulation environment written in MATLAB and incorporating the Aerosim Blockset for Simulink by Unmanned Dynamics [22] was used. A 6 degree-of-freedom nonlinear rigid body aircraft model with aerodynamic

coefficients of a Navion aircraft from [11] was "flown" in simulation to generate the "truth" data. The truth was then corrupted with noise to simulate the various system errors. Each of the values of noise used in the simulation is given in Table II. A white noise process is denoted as $WN(\sigma)$ and a first-order Gauss-Markov process will be referred to as $GM(\sigma, \tau)$ where σ is the standard deviation and τ is the correlation time.

GPS pseudorange and pseudorange rate noises were modelled as a sum of Gauss-Markov processes for correlated noise plus white noise for measurement noise as in [23]. Assuming the availability of L1 and L5 measurements, it was assumed that the majority of ionospheric error was reduced by cancelling the error with the use of the second frequency. It was assumed that tropospheric error was reduced by a tropospheric delay model. The sample rate of the GPS pseudorange and pseudorange rates was 1 Hz. For the GPS satellite constellation, a changing 24-satellite optimized GPS constellation from [19] was used.

The IMU accelerometer and gyroscope errors were modelled as a random bias (Gauss-Markov process) [24] plus white noise. The values given in Table II for the noise and bias were measured values from a laboratory test of a Crossbow MicroNAV at Queensland University of Technology, Brisbane. The sample rate for the IMU measurements was 100 Hz. Admittedly, this generic error model is only an approximation of the sum total of a wide variety of error sources within the IMU.

The ADM was a 6-Degree-of-Freedom nonlinear rigid body model [10]. The ADM errors considered were control input, aerodynamic coefficient, mass and inertia, centre of gravity, gravity and wind as given. The sample rate for the control input measurements was 100 Hz with values for control input noise of WN (0.02°) in Table II obtained from [25]. The ADM accuracy is limited particularly by the aerodynamic coefficient uncertainty and the unknown and nondeterministic wind environment. Reference [5] states that the aerodynamic coefficients can typically be known up to 10% of their true values. The aerodynamic coefficient errors were modelled as independent first-order Gauss-Markov processes where the time constants were chosen to give some random variation. The errors for throttle, mass, inertia and centre of gravity were chosen based on judgement. The wind conditions and gravity error were chosen arbitrarily.

The other major source of error in the ADM is that the overall position, velocity and attitude errors grow with time, (as in an INS), since the information is derived from integration. These errors limit the benefits to be gained from the ADM.

TABLE II
SIMULATION PARAMETER VALUES

Parameter	Value
GPS	
Ephemeris	*GM* (2.4 m, 1800 s)
Ionosphere (L1-L5)	*GM* (0.4 m, 1800 s)
Troposphere	*GM* (0.4 m, 3600 s)
Multipath (Code)	*GM* (0.25 m, 600 s)
Receiver Noise (Code)	*WN* (0.1 m)
Multipath (Carrier)	*GM* (0.048 m, 600 s)
Receiver Noise (Carrier)	*WN* (0.0019 m)
Total L1-L5 1σ Pseudorange Noise	2.47 m
GPS Receiver Clock	Typical Crystal Oscillator [26]
GPS Antenna Elevation Mask	5 °
IMU	
p gyro Noise	*WN* (0.53 °/s)
q gyro Noise	*WN* (0.45 °/s)
r gyro Noise	*WN* (0.44 °/s)
x accel Noise	*WN* (0.013 m/s^2)
y accel Noise	*WN* (0.018 m/s^2)
z accel Noise	*WN* (0.010 m/s^2)
p gyro Bias	*GM*(0.0552 °/s, 300 s)
q gyro Bias	*GM*(0.0552 °/s, 300 s)
r gyro Bias	*GM*(0.0552 °/s, 300 s)
x accel Bias	*GM*(0.0124 m/s^2, 300 s)
y accel Bias	*GM*(0.0124 m/s^2, 300 s)
z accel Bias	*GM*(0.0124 m/s^2, 300 s)
ADM	
Coefficients	*GM* (10 %, 120 s)
Control Inputs	*WN* (0.02 °) aileron, rudder, elevator. *WN* (2%) throttle setting.
Centre of Gravity Error [x, y, z]	[0.03, 0.03, 0.03] m
Mass Error	2% of true
Moment of Inertia Error, [J_x, J_y, J_z, J_{xz}]	2% of true
Environmental	
Wind [North, East, Down]	[10 kn, 10 kn, 2 kn] mean, with Von Karman turbulence model
Gravity Error 1σ	36 μg

As shown in Fig. 4 an APV approach was simulated starting from an assumed Final Approach Fix (FAF)

waypoint at 1500 feet altitude and descending at a rate of between 350-500 ft per min in the vicinity of Brisbane airport, Australia with an assumed Decision Height (DH) of 375 ft.
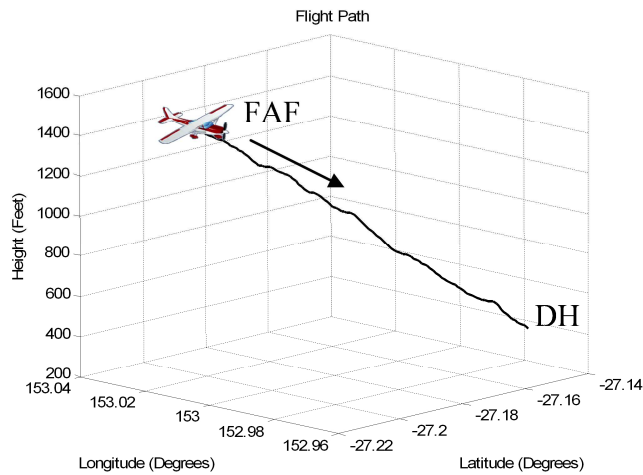

Fig. 4. Simulated APV approach.

The results for the GPS-IMU-ADM EKF in detecting a 0.5 m/s ramp fault will be presented next.

A. Detection of 0.5 m/s Ramp Fault

A 0.5 m/s ramp fault was placed on the pseudorange of the "most difficult satellite to detect" starting at 25 seconds into the simulation. 0.5 m/s was chosen because it was the smallest value of ramp fault which caused the positioning error to exceed the alert limits before the DH was reached.

As shown in Fig. 5 there was an average of 7 satellites available however the number of satellites varied due to aircraft motion, occasionally dropping down to 6. This occurred as the "pilot" maneuvered the aircraft to keep it on course, causing some satellites at low elevation to drop below the elevation mask at times. Fig. 5 can be used to compare with the protection level results to observe the effect which the number of visible satellites available had on protection levels.
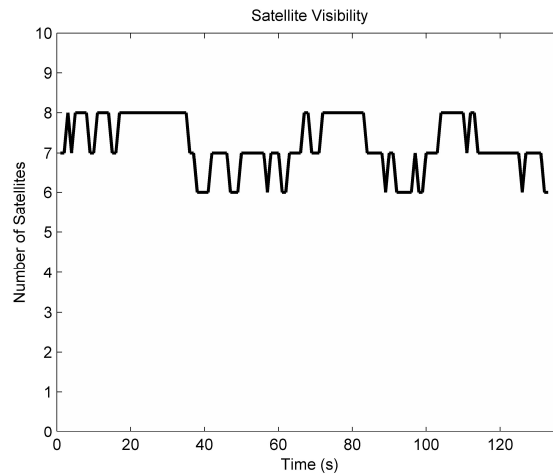
Fig. 5. Number of visible satellites above the elevation mask.

To compare the protection levels, Fig. 6 compares the HPL of the GPS-IMU-ADM EKF (labeled "GPS-IMU-ADM EKF" in the legend of Fig. 6) with a "snapshot" implementation of the NSS method using GPS alone (labeled "HPL GPS") against the NSS method with a GPS-IMU EKF (labeled "GPS-IMU EKF"). Firstly, it can be seen that the HPL for the GPS was higher (approximately 10 to 25 m) and more dependent upon the satellite geometry than the HPL for the GPS-IMU EKF or GPS-IMU-ADM EKF. Fig. 7 shows similar results, except the VPL GPS exceeds the VAL temporarily from Time 40 s onwards. By comparing with Fig. 5 this was the times when the number of visible satellites drop to six. This shows the benefits of using a filtered implementation over snapshot implementations, particularly in times of low satellite visibility since the GPS-only fault detection performance is more dependant upon good satellite geometry than the filtered cases. There was calculated to be an average reduction over the whole approach of 49.9% in HPL and 57.9% in VPL with GPS-IMU EKF, over GPS alone. This shows that compared to the GPS-only implementation, a reduction in protection level is possible due to greater confidence in the position estimates by fusing the GPS with the IMU and ADM in EKFs.

Now to evaluate whether fusing the IMU with the ADM has any benefit it can be seen in Fig. 6 and Fig. 7 that the HPL and VPL of the GPS-IMU-ADM EKF were only a little lower than GPS-IMU EKF. This was calculated to be an average reduction of 1.4% in HPL and 5.3% in VPL over GPS-IMU EKF. This shows that fusing the IMU with ADM achieves only a small reduction in protection levels.
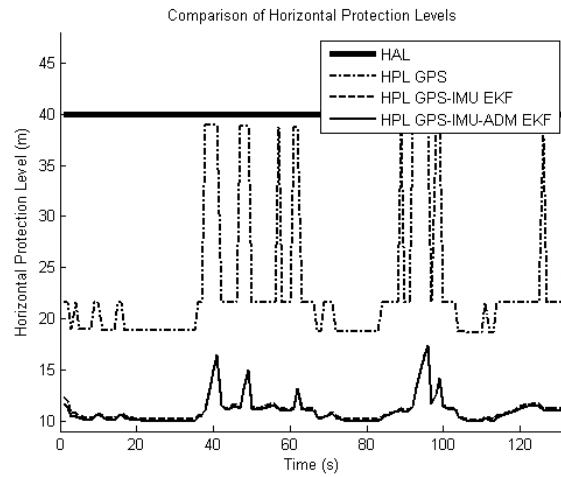
Fig. 6. Comparison between the HPL of the GPS, GPS-IMU EKF and GPS-IMU-ADM EKF.
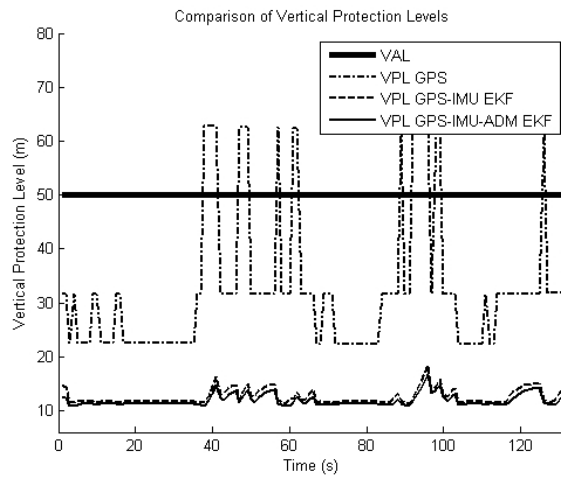

Fig. 7. Comparison between the VPL of the GPS, GPS-IMU EKF and GPS-IMU-ADM EKF.

To consider whether or not the fault was detected and how long it took, Fig. 8 plots the test statistic and threshold with Horizontal Position Error (HPE) and HPL for the GPS-IMU-ADM EKF. As indicated by the arrows the fault was detected before the HPE exceeded the HPL. This shows that the system is capable of detecting the fault before the position error exceeds the protection level and well before the error would exceed the alert limit of 40 m (Table I). However this one test case does not prove that the probability of missed detection requirement is met. Extensive Monte Carlo simulation is required to verify that the HPL meets the P_{md} requirement and this is left for further work.
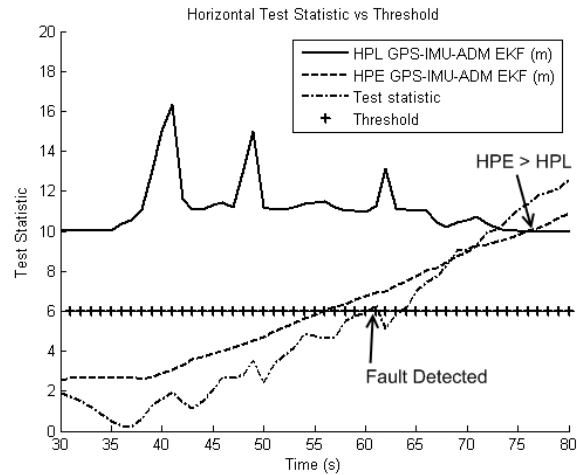
Fig. 8. *Horizontal test statistic versus threshold of the GPS-IMU-ADM EKF.*

To summarize the fault detection results for all systems, Table III compares *Time to Detection* which was the time taken to detect the fault from the onset of the fault, against *Time to NSE > PL* which was the time it took for the Navigation System Error (NSE) to exceed the protection level (PL). In Table III, H and V indicate the horizontal and vertical directions, respectively. By comparing the *Time to Detection* with the corresponding *Time to NSE > PL* , it can be seen that the 0.5 m/s ramp fault was detected by all systems before the position error exceeds the protection level. However it was detected earlier in the filtered systems than the GPS-only case. By comparing the smallest *Time to Detection* for the GPS (56 seconds for the vertical case "GPS V"), with the smallest time for the GPS-IMU EKF and GPS-IMU-ADM EKF (35 seconds each, for the horizontal cases), the fault is detected by the filtered systems approximately 21 seconds (or 37%) sooner than the GPS-only case.

Now comparing the horizontal cases of the GPS-IMU-ADM EKF with the GPS-IMU EKF, the *Time to Detection* are the same (35 s) for both, and the fault was detected only one second sooner in the vertical case for the GPS-IMU-ADM EKF than for the GPS-IMU EKF (35 s and 36 s, respectively). This shows that there was no significant reduction in *Time to Detection* by fusing the IMU with the ADM.

TABLE III
0.5 M/S RAMP FAULT DETECTION TIMES

	Time to Detection (s)	Time to NSE > PL (s)
GPS H	59	86
GPS V	56	95
GPS-IMU EKF H	35	52
GPS-IMU EKF V	36	46
GPS-IMU-ADM EKF H	35	50
GPS-IMU-ADM EKF V	35	41

B. Comparison of Average Protection Levels over a Day

To assess the protection level performance over a 24-hour period of changing satellite geometries for the one flight path shown in Fig. 4, the test was repeated 70 times where only the satellite geometry was varied each time at 20 minute intervals. Only 70 runs were chosen due to our simulation environment's limitations, however, this scenario may be thought of as an aircraft conducting an APV approach every 20 minutes, assuming each aircraft flies exactly the same path in the same conditions. Over all 70 simulation runs, the number of visible satellites was observed to vary anywhere from 6 to 10, with the average being 8.

Fig. 9 and Fig. 10 show the HPL and VPL which has been averaged over the 70 simulation runs. As can be seen in Fig. 9, the HPL for the GPS was approximately 11 m higher than for the filtered cases and in Fig. 10 the GPS VPL was approximately 20 m higher. This was calculated to be an average reduction in HPL and VPL of 48.2% and 54.5% with GPS-IMU EKF, over GPS alone. To consider the availability of fault detection on this one simulated approach it was calculated that 85.5% of the time the GPS HPL or VPL exceeded the HAL or VAL requirements. In contrast, the availability of fault detection was 100% for both the GPS-IMU EKF and GPS-IMU-ADM EKF. Although this is not an extensive availability analysis, the results show that fusing GPS with a low-cost IMU can achieve greater availability than GPS-only schemes.

To consider the effect of including the ADM in the architecture, the HPL of the GPS-IMU-ADM EKF was calculated to be 2.7% lower than the GPS-IMU EKF and the VPL was 5.6% lower. This small reduction in HPL due to fusion of the IMU with the ADM may contribute to an increase in availability of

the fault detection function, however, without extensive Monte Carlo simulation the overall significance of this cannot be determined. Such small reductions in protection level may be more significant only if the performance requirements are much tighter or satellite visibility is poor.
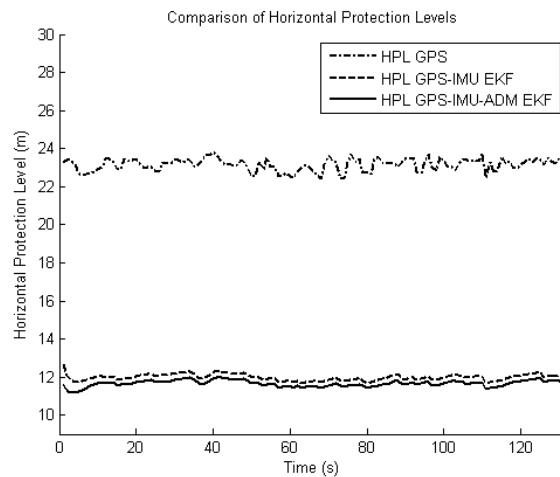

Fig. 9. Comparison between the average HPL of the GPS, GPS-IMU EKF and GPS-IMU-ADM EKF.
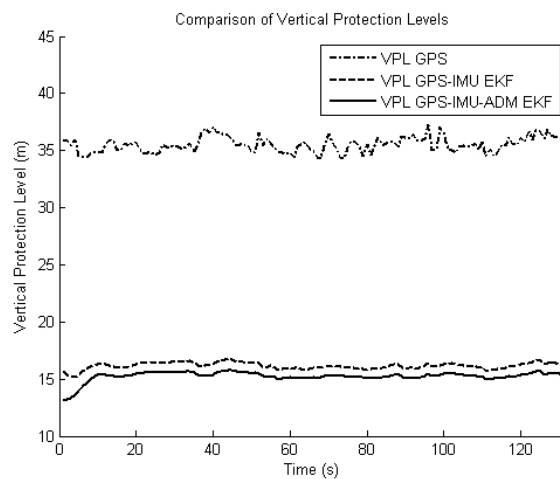

Fig. 10. Comparison between the average VPL of the GPS, GPS-IMU EKF and GPS-IMU-ADM EKF.

In summary, whilst the fusing of the ADM with the IMU was shown to reduce the protection levels, this reduction may not be large enough to justify including an ADM in practical systems for general aviation considering the added complexity of the GPS-IMU-ADM EKF architecture over a GPS-IMU EKF. The

performance improvements are limited due to the new information that the ADM brings to the system being in the form of derivatives, which always have a component of error growing with time. Furthermore, the incorporation of the ADM may not be cost-effective in practical systems for general aviation since currently the use of aircraft dynamics and sensors to measure pilot inputs is not common.

V. Conclusion

This paper investigated augmenting GPS with a low-quality MEMS IMU and ADM fused together in a bank of EKFs using a NSS fault detection scheme. This was called the GPS-IMU-ADM EKF. Unlike past ABAS designs, the use of EKFs in a closed-loop configuration with a low-cost IMU and ADM were considered.

By simulation of a general aviation aircraft on an APV approach, the performance of the GPS-IMU-ADM EKF in detecting a ramp fault on one GPS pseudorange measurement was evaluated. By comparison with a GPS-only snapshot implementation of the NSS method it was observed that protection levels were reduced by 51% and the ramp fault was detected 37% sooner than the GPS-only implementation. This shows a potential benefit in using a filtered approach over a snapshot implementation since an improvement in fault detection availability may be gained.

The effect of including the ADM was evaluated by comparing the GPS-IMU-ADM EKF with a GPS-IMU EKF. The GPS-IMU-ADM EKF gave a 2.7% reduction in horizontal protection level and 5.6% in vertical protection level as compared to a GPS-IMU EKF (averaged over 70 different satellite geometries in a 24 hour period) for a single APV approach. Even though the incorporation of the ADM showed a small reduction in protection levels (which may result in an increase in fault detection availability), this reduction may not be large enough to justify the effort and cost of including an ADM in practical systems.

Further research could be made to assess fault exclusion performance, verify that the protection levels meet the statistical requirements through Monte Carlo simulation and investigate the performance over

different fault conditions and scenarios. One potential use for affordable ABAS for general aviation may be to enhance existing GPS-only fault detection solutions or to help overcome any outages in augmentation systems such as GRAS. Countries such as Australia which currently do not have an augmentation solution for general aviation could especially benefit from the economic and safety benefits of satellite navigation-based APV approaches.

REFERENCES

[1]   Y. C. Lee, R. Braff, J. P. Fernow, D. Hashemi, M. P. McLaughlin and D. O'Laughlin, "GPS and Galileo with RAIM or WAAS for vertically guided approaches," in ION GNSS, Long Beach, CA, 2005.

[2]   J. Diesel and S. Luu, "GPS/IRS AIME: calculation of thresholds and protection radius using chi-square methods," in ION GPS-95, 1995.

[3]   M. Brenner, "Integrated GPS/Inertial fault detection availability," in ION GPS 95, 1995.

[4]   R. S. Y. Young and G. A. McGraw, "Fault detection and exclusion using normalized solution separation and residual monitoring methods," Navigation: The Journal of the Institute of Navigation, 2003.

[5]   M. Koifman and I. Y. Bar-Itzhack, "Inertial navigation system aided by aircraft dynamics," IEEE Transactions on Control Systems Technology, vol. 7, 1999.

[6]   C. Eck, H. P. Geering and S. C. Bose, "Model based INS/GPS navigation," in 7th Saint Petersburg International Conference on Integrated Navigation Systems, St. Petersburg, Russia, 2000.

[7]   K. P. A. Lievens, J. A. Mulder and P. Chu, "Single GPS antenna attitude determination of a fixed wing aircraft aided with aircraft aerodynamics," in AIAA Guidance, Navigation and Control Conference, San Francisco, California, 2005.

[8]   W. Ely, "GRAS development, approval and implementation in Australia," Sydney: University of New South Wales, 2006.

[9]   J. Farrell, R. Anoll, and E. McConkey, "IMU Coast: Not a Silver Bullet," in ION 55th Annual Meeting Cambridge, MA, 1999.

[10] B. L. Stevens and F. L. Lewis, Aircraft Control and Simulation. Toronto: John Wiley & Sons, 1992.

[11] R. C. Nelson, Flight Stability and Automatic Control, 2nd ed. Singapore: WCB/McGraw-Hill, 1998.

[12] D. H. Titterton, J. L. Weston and Institution of Electrical Engineers., Strapdown Inertial Navigation Technology, 2nd ed. Stevenage, U.K.: Institution of Electrical Engineers American Institute of Aeronautics and Astronautics, 2004.

[13] S. J. Julier, "Process models for the navigation of high-speed land vehicles," in Department of Engineering Science: University of Oxford, 1997.

[14] S. J. Julier and H. F. Durrant-Whyte, "A horizontal model fusion paradigm," in The Proceedings of the SPIE AeroSense Conference: Navigation and Control Technologies for Unmanned Systems Orlando, FL, USA, 1996.

[15] R. G. Brown and P. Y. C. Hwang, Introduction to Random Signals and Applied Kalman Filtering, 2nd ed. New York: John Wiley & Sons, 1992, p. 263.

[16] J. H. Kim, S. Sukkarieh, E. M. Nebot, and J. Guivant, "On the Effects of Using Heading Information During Inflight Alignment of Low-Cost IMU/GPS Integrated System," in International Conference of Field and Service Robotics, Finland, 2001.

[17] "ICAO Standards and Recommended Practices Annex 10 - Aeronautical Telecommunications - Volume 1.," International Civil Aviation Organisation.

[18] K. L. Van Dyke, "Use of stand alone GPS for approach with vertical guidance," in ION National Technical Meeting 2001, Long Beach, CA, 2001.

[19] "Minimum Operational Performance Standards for Global Positioning System/Wide Area Augmentation System Airborne Equipment," Radio Technical Commission for Aeronautics Inc., Washington DO-229D, 2006.

[20] "Minimum Operational Performance Standards for GPS Ground-based Regional Augmentation System Airborne Equipment," Radio Technical Commission for Aeronautics Inc., Washington DO-310, 2008.

[21] "CRC Handbook of Tables for Probability and Statistics ", W. H. Beyer, Ed.: Chemical Rubber Company, 1968.

[22] http://www.u-dynamics.com/aerosim/, 1 July, 2008.

[23] J. Rankin, "GPS and differential GPS: an error model for sensor simulation " in Proceedings of the IEEE Position Location and Navigation Symposium, 1994.

[24] Y. Bar-Shalom, X. R. Li and T. Kirubarajan, "Estimation with Applications to Tracking and Navigation," John Wiley & Sons, Inc., 2001, p. 497.

[25] V. Klein and E. Morelli, Aircraft System Identification: Theory and Practice. Virginia: American Institute of Aeronautics and Astronautics, Inc. , 2006, p. 296.

[26] R. G. Brown and P. Y. C. Hwang, "Introduction to Random Signals and Applied Kalman Filtering," 2nd ed New York: John Wiley & Sons, 1992, p. 430.

[27] J. Blanch, T. Walter, and P. Enge, "Position Error Bound Calculation for GNSS using Measurement Residuals," *IEEE Transactions of Aerospace and Electronic Systems,* vol. 44, 2008.